Received: November 28, 2024. Revised: January 21, 2025. 589

International Journal of
Intelligent Engineering & Systems

http://www.inass.org/

A Tri-elliptic Shaped Microstrip Patch UWB Antenna for Chipless RFID Tags

Ghazi Bin Wan Mohamed[1] A. K. M. Zakir Hossain[1]* Nurulhalim Bin Hassim[1]
Fahmida Hossain[1] Muhammad Ibn Ibrahimy[2]

[1]Fakulti Teknologi dan Kejeruteraan Elektronik dan Komputer (FTKEK), Universiti Teknikal Malaysia Melaka (UTeM), Melaka, Malaysia
[2]Faculty of Engineering, Dept. of Electrical and Computer Engineering (ECE), International Islamic University Malaysia (IIUM), Gombak, Malaysia
* Corresponding author's Email: zakir@utem.edu.my

Abstract: This article presents a tri-elliptic microstrip patch antenna for ultra-wide band (UWB) chipless RFID (CRFID) applications. The simple and compact structure consists of three elliptical patches that are optimized for bandwidth (BW) enhancement. The antenna is fabricated on a Rogers RT 5880 substrate with a compact size of 36.8×28 mm^2 and has a partial ground plane (PGP) for wideband response. Both simulation and experimental results show a good agreement, hence confirming its high efficiency and omnidirectional radiation characteristics**.** It operates in the UWB frequency band from 3.67 to 10.5 GHz, showing a measured VSWR < 2 bandwidth of 6.83 GHz, a peak realized gain of 5.4 dBi, and a radiation efficiency greater than 94%. Further, the gain-to-aperture ratio (GAR) is calculated. It is found that the proposed antenna outperforms most of the existing CRFID tag antennas with 0.52 dBi/cm^2. In addition, the antenna is tested in anechoic chamber and different multipath line of sight (LOS) scenarios for far field radiation pattern and wireless communication validation. Moreover, the antenna is attached with a 9-bit truncated-C multi-resonator (TCMR) to demonstrate its capabilities of encoding and decoding a wireless bit sequence of 'All Present' (111111111) even in the presence of path loss and attenuation. With proper implementation and adaptation to innovative and wearable technologies, this proposed design can become a foundational model for a suitable candidate in logistics, healthcare, and wearable applications, providing a reliable solution for next-generation UWB CRFID systems.

Keywords: Ultra-wide band, Chipless RFID, Partial ground plane, Realized gain, Multi-resonator, Bit sequence.

1. Introduction

Chipless Radio Frequency Identification (CRFID) technology has developed as a favourable alternative to traditional RFID systems, primarily due to its cost-effectiveness by eliminating the integrated circuit (IC) in RFID tags. The chipless RFID significantly reduces the manufacturing costs, making it a potential candidate for a wide range of industries, from logistics and inventory management to healthcare and security [1, 2]. However, the success of CRFID systems heavily depends on the performance of the antennas on board, which play a critical role in the system's ability to detect the object/product. Fig. 1 illustrates the conventional CRFID system diagram [3]. As most of the CRFIDs operate in the 3.1 GHz - 10.7 GHz (ultra-wideband) region, the need for compact, high-performance, ultra-wideband (UWB) antennas is necessary [4]. This has led to significant research focused on improving antenna designs, with the ultimate goal of creating smaller, more efficient, and cost-effective solutions for chipless RFID systems. Moreover, among many other designs proposed in recent years, these antennas can operate over a wide band of frequencies [5], which is essential for chipless RFID systems where spectral signatures are used to encode information. Such a wide bandwidth (BW) facilitates not only accurate tag detection but also the system's capability, in the multitude of tags in complex environments, to handle such tags even with signal

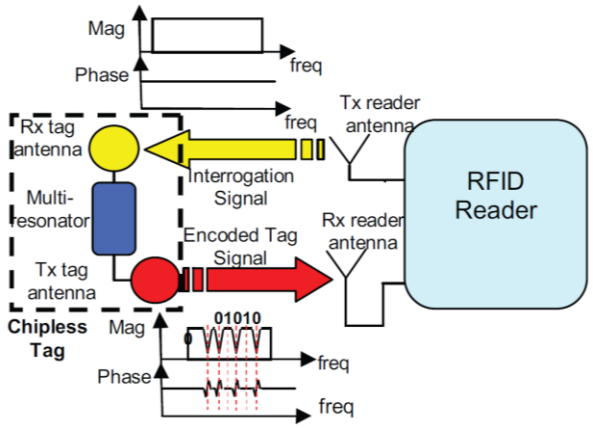

Figure. 1 Conventional retransmission based CRFID system [6]

reflection and interferences that might otherwise degrade their performance.

One of the major contributions in this direction is the flower-shaped monopole antenna, designed by [7], for operation over the BW from 1.2 to 3 GHz. This 50 × 76 mm² sized antenna has a realized gain (RG) of 4 dBi and operates with an efficiency ranging from 80% to 96%, which makes it strong in applications where there has to be a trade-off between size and performance. The employment of FR-4 as a substrate (ε_r = 4.4) gives structural rigidity, but its rigid nature may limit its application to flexible environments such as wearable technology. Moreover, this design does not demonstrate the UWB performance at the BW mere 1.8 GHz and also not operates with the UWB frequency range. Also, the antenna is comparatively bigger in size.

Compared to the rigid structures, flexible antennas attract more and more popularity due to their versatility in different scenarios, especially in healthcare and logistic applications, due to the rising demand for dynamic and deformable tags. In [8], the authors proposed a 32 × 30 mm² dimension Defective Grounded Circular Monopole (DGCMP) antenna that resonates over a much wider BW from 3 to 11.1 GHz. The RG for this antenna varies between 2 and 4.5 dBi. This has been made possible by using Taconic TLX-0 as a substrate with ε_r = 2.45. The efficiency of this design was, however, not given, which leaves some doubt as to its overall performance, especially in environments with a high signal attenuation. Still, this design is a significant advance toward building the flexible UWB antennas for chipless RFID systems due to their compact form factor and wide BW. Another proposal is made in [9] used the inset feed microstrip patch antenna on RO4030C substrate to create another chipless RFID tag-sensor antenna measuring 41.8 × 38.5 mm². Operating between 2.34 - 2.42 GHz, this antenna achieves a good, RG of 6 dBi. However, it is evident that the antenna has a narrow BW. Also, the authors have not presented any antenna efficiency which makes it difficult to assess the performance of this proposed antenna.

A compact design was proposed in [10] where the authors have introduced a keyhole-shaped monopole antenna that operates over a BW of 3.59 to 10.28 GHz. Measuring just 32 × 20 mm², this antenna achieves a RG of 4 dBi and operates with an efficiency between 96% and 99%, making it one of the most efficient designs in this review. The use of Rogers RT3003 (ε_r = 3.0) as the substrate ensures flexibility, which is particularly useful in environments requiring deformable or wearable RFID tags. However, the proposed work is done in simulation only and not tested on any multi-resonators tag(s) which still creates doubt over the real-world performance of this antenna for CRFID application. Moreover, the authors in [11] have proposed a low profile 20-bit CRFID tag with CPW feed I-slotted UWB planar antenna with a comparatively small dimension of 27.7 × 29.9 mm2 on rigid RF-4 substrate. The antenna works within the frequency range of 3-12 GHz occupying the whole UWB region. The antenna exhibits a remarkable peak RG of 6dBi and a x-polar level of below -15 dB. Also, the antenna shows a good omni-directional far-field pattern. Even though the antenna shows good gain with a compact size, the authors have not disclosed the antenna efficiency which is an important parameter for performance assessment.

In [12] another approach in shown for the miniaturization and performance improvement of CRFID antenna. In this proposal the authors have presented an interdigital capacitor meander line antenna with dimensions of 53 × 86 mm² that operates over a BW of 3.4 to 10 GHz. The use of RO4350B as a substrate indicates that the design was likely optimized for high-frequency and low-loss applications. While the relatively large size of this antenna may limit its application in space-constrained environments and although its realized gain and efficiency were not specified. In the same vain, [13] has proposed a circular disc monopole patch antenna that can produce the circular polarization beam. In this proposed design, the ground plane is modified as defected ground structure to increase the BW that works between 1.88 - 6.04 GHz. The antenna as a dimension of 55 × 30 mm2 with omni-directional radiation pattern. Yet, the proposed method does not disclose the significant information on the RG and the antenna efficiency, makes it difficult evaluate further implementation ability for large scale deployment. The proposal in [14] reveals a design intended to explore the aspect of CRFID tagging and temperature

sensing by utilizing the circular spiral resonator and microstrip planar stepped patch monopole UWB antenna. The antenna size is relatively small with 33 × 30 mm2 only and the operational BW is within the UWB region from 3 to 18 GHz with omni-directional far field pattern. Even though the antenna exhibits a very wide BW of 15 GHz, yet the authors have not provided the gain and the antenna efficiency information which hinders the future applicability and development of this particular antenna.

One more design in [15] is explored that utilized an annular slot antenna, which operates in the 2.5 to 5 GHz range. This design of 30 × 40 mm² realizes a gain of -3.9 dBi. Comparatively, the gain of these designs is rather low. Due to its simplicity and low cost, the FR-4 substrate material (ε_r = 4.4) is a good candidate for those applications where low cost is an important constraint, and high performance is not of vital interest. This annular-slot geometry is particularly useful in applications where omnidirectional radiation patterns are desired, although the low gain (due to low efficient substrate) may restrict its range and effectiveness in some RFID applications. Another proposal is made in [16] with a dual-polarized monopole involving the spiral linearly slotted resonators (SLSR) designed to operate between 2 and 5.1 GHz. This antenna, comparatively bigger in size measuring 40 × 50 mm², achieves gains of 2.3, 3.5, and 5 dBi at corresponding frequency points within the BW, offering a good solution for multi-band applications. The performance of the antenna is further enhanced by the use of Rogers 5880 as the substrate with ε_r = 2.0 to minimize the signal loss. This design is very beneficial to the environment in which high-frequency operation over a number of bands is required, like logistics and supply chain management, where a large frequency span has to be operated so as to handle different RFID tags. Still the antenna is not fully operating in the UWB region and also the efficiency in not mentioned as it's a very important parameter for the antenna quality assessment.

In [17] the authors presented a step-shaped rectangular patch antenna with small size of 39.6 × 25 mm², designed to operate in the 5 to 12 GHz range. This antenna has a RG of 8 dBi and efficiency of 90%, which is one of the best among the reviewed designs here. The use of RT Duroid 5880 (ε_r = 2.2) as the substrate helps to minimize the loss at high frequencies and hence it's more suitable for long-range applications where high gain is needed. This design proves that novel geometrical designs can bring high-performance enhancement, though the stiff substrate can prohibit its application in flexible or wearable RFID systems. Similarly, another high-gain design in [18], where the authors have proposed a stair-step patch antenna that operates between 3 and 6 GHz. This large antenna, measuring 67.6 × 107 mm², achieves gains ranging from 2.34 to 4.08 dBi. While its size may limit its use in compact applications, the use of RT/Duroid 5870 as the substrate suggests it is optimized for high-performance environments where signal integrity is critical, such as industrial settings or fixed infrastructure. Similarly, an egg-shaped monopole antenna is designed in [19] that offers a flexible design, with dimensions of 170 × 120 mm². Operating from 0.9 to 2.9 GHz, this antenna really offers a novel geometry for the improvement of the BW, although its RG wasn't given. Its flexible substrate, PET, makes sure it can be employed in various dynamic environments, making it a very strong candidate for RFID applications where adaptability is needed. However, the antenna itself is huge in size which would hinder its attached ability to cooperatively smaller object/products.

In similar way [20] has developed a tree-profile shape UWB antenna with a size of 27 × 40 mm², operating over an impressive BW of 2.72 to 11.1 GHz. With a RG of 4.2 dBi and an efficiency range of 80% to 96%, this design is optimized for UWB RFID applications. The use of Rogers RT/Duroid 3003 enhances its performance, making it good candidate for environments where both compact size and high efficiency are required. Recently, [21] utilized a unique way of antenna integration for CRFID ammonia gas tag-sensor. The proposed method uses a cascaded dual antenna prototype consisting of a conventional rectangular microstrip monopole antenna and a planar inverted-F antenna (IFA). The monopole works within 3.8-6.9 GHz whereby the IFA works as a narrow band centred at 2.65 GHz and they both are fabricated on the rogers 5880 rigid substrate. The IFA exhibits a low gain of 2 dBi whereas the monopole shows a comparatively higher average gain of 3.3 dBi. However again, the authors do not disclose the antenna efficiency which is very significant for antenna performance. Table. 1, summarize the Comparison between existing microstrip antennas used in CRFID Tags with the proposed antenna.

From Table 1, it can be seen that only a few proposals reveal the antenna efficiency. Moreover, some perform well in terms of the BW but fail in efficiency and gain. In contrast, some antenna sizes are relatively small, but the RG is poor. Furthermore, some exhibit good gain, but the size is larger, resulting in a poor gain-to-aperture ratio (GAR). Keeping these issues in mind, this paper proposes a

Table. 1. Comparison between existing microstrip antennas used in CRFID Tags

Ref	Size (mm^2)	BW (GHz)	Effi (%)	RG (dBi)	GAR dBi/cm^2
[7]	50 × 76	1.2-3	80	4	0.11
[8]	32 × 30	3-11.1	NA	4.5	0.47
[9]	41.8 × 38.5	2.34-2.42	NA	6	0.37
[10]	32 × 20	3.6-10.3	96	4	0.62
[11]	27.7 × 29.9	3-12	NA	6	0.72
[12]	53 × 86	3.4-10	NA	NA	-
[13]	55 × 30	1.88-6.04	NA	NA	-
[14]	33 × 30	3-18	NA	NA	-
[15]	30 × 40	2.5-5	NA	-3.9	-0.33
[16]	40 × 50	2-5.2	NA	5	0.25
[17]	74.6 × 25	5-12	90	8	0.43
[18]	67.6 × 107	3-6	NA	4.08	0.06
[19]	170 ×120	0.9-2.9	NA	NA	-
[20]	40 ×27	2.7-11.1	80	4.2	0.39
[21]	68 × 36	3.8-6.9	NA	3.3	0.13
This work	**36.8 × 28**	**3.67 – 10.5**	**94**	**5.4**	**0.52**

*Effi = Antenna Efficiency, NA = not available

planar microstrip tri-elliptic-shaped UWB antenna on a Rogers 5880 substrate, which outperforms most other proposals with a better GAR value. This indicates this proposed antenna is comparatively small in size with relatively high RG. In addition, this antenna covers almost the entire UWB range with high antenna efficiency and radiation efficiency. To prove its significance and applicability, this antenna is tested in an anechoic chamber for its far-field pattern and in various orientations for multipath line-of-sight (LOS) wireless communication. Additionally, this antenna is deployed with the existing multi-resonator for its suitability in CRFID applications.

2. Tri-elliptic CRFID antenna design

Fig. 2. Illustrates the final diagram of the proposed antenna. Fig. 2(a) and (b) comprise the top and the bottom view of the antenna.

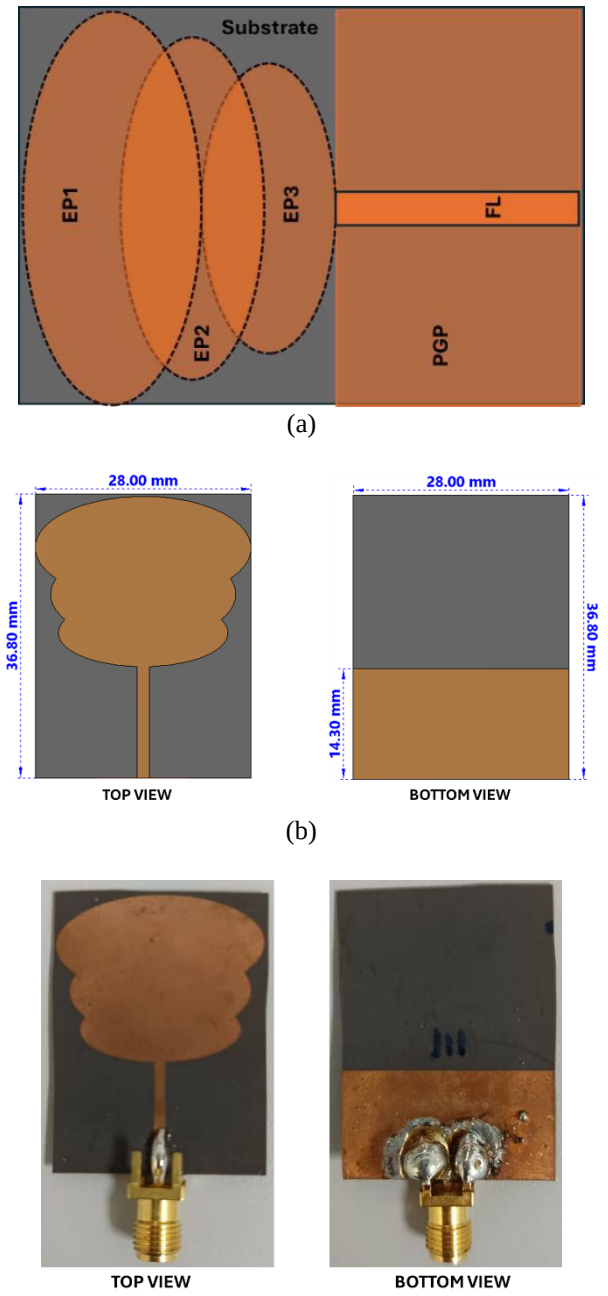

Figure. 2 Proposed antenna layout and top & bottom view: (a) Layout, (b) Top and Bottom View (Simulated), and (c)Top and Bottom View (Fabricated)

The antenna is a microstrip structure combined with three different size elliptical shaped patches. The elliptic patch 1 (EP1) is estimated by utilizing the Eqs. (1) to. (3) [22], where f0 is the resonant frequency, C0 is the speed of light in free space, a and b is the major and the minor axis' radius of the elliptical patch respectively. The initial approximation in the relation of the size of the patch EP2:EP1 is 3:5. Moreover, the ratio of the size of the EP3 and EP2 is 4:5. So, the final optimized dimensions of the three elliptical patches are shown in Table 2. The patch EP2 top upper side starts at the centre of the EP1.

Table. 2. Major and minor axis dimensions

Patch	Major axis (mm)	Minor axis (mm)
EP1	14	9.5
EP2	12	8.2
EP3	11	5.3

In similar way, the EP3's top upper side starts at the centre of the EP2 (See Fig. 2(a)). The bottom side of the patch EP3 is connected with the microstrip 50 Ω transmission line (TL) feed with a length of 14.4 mm. The width of the TL is 1. The bottom patch, the

$$f_0 = \frac{1.8412C_0}{2\pi r_{ref}\sqrt{\varepsilon_{eff}}} \quad (1)$$

$$r_{reff} = \sqrt{\frac{ab}{\pi}} \quad (2)$$

$$\varepsilon_{eff} = \frac{\varepsilon_r+1}{2} + \frac{\varepsilon_r-1}{2}\left(1 + 12\frac{h}{r_{ref}}\right)^{-0.5} \quad (3)$$

ground plane is truncated to 14.4mm in length to create a partial ground plane (PGP) for wide band response and can be seen from Fig. 2(c). Finally, the antenna is fabricated on PCB Rogers RT 5880 ($\varepsilon_r = 2.2,\ \tan\delta = 0.0009, h = 0.508$ mm) and soldered with the 50 Ω SMA connector. Fig. 2(d) and (e) illustrate the top and the bottom view of the fabricated tri-elliptic antenna. The final antenna dimension is obtained as $36.8 \times 28 \times 0.508$ mm^3.

Fig. 3(a) discloses the deign steps of the proposed antenna which is simulated using the 3-D electromagnetic simulation CST MWS 2022. Moreover, the simulated S-parameter (S11) results of the different steps are accumulated in Fig. 3(b). At first step, one elliptical patch, EP1 is modelled and connected with the microstrip transmission line. The full ground plane (FGP) is kept for this simulation. It is seen from the step 1's S11 response (red) that there is a small resonance point at 8 GHz crossing just below -10 dB. At the second step one more patch (EP2) is added in the design while keeping the FGP to see the effect on the S11 response (green). It is seen that there is a visible resonance around 8.25 GHz reaching -20 dB. However, the BW is narrow and still not covering the UWB ranges. In third step, one more patch (EP3) is added to the design and still no changes are done on the FGP. It can be seen from the S11 response (blue) that the resonance is shifted a little bit from 8.25 GHz to 8.3 GHz. Moreover, there is a potential broadband resonance appearing, however, not touching -10 dB around 10 GHz - 11GHz.

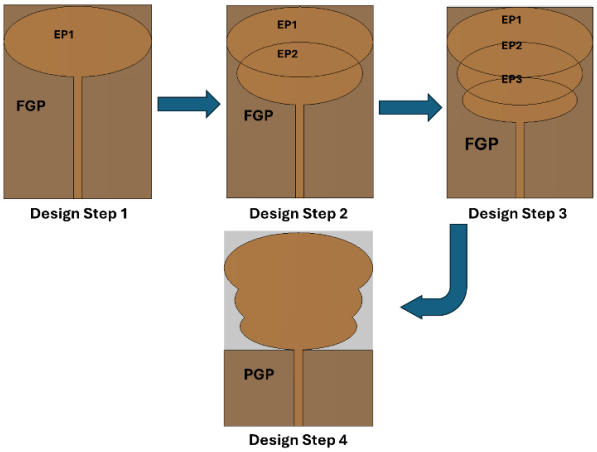

(a)

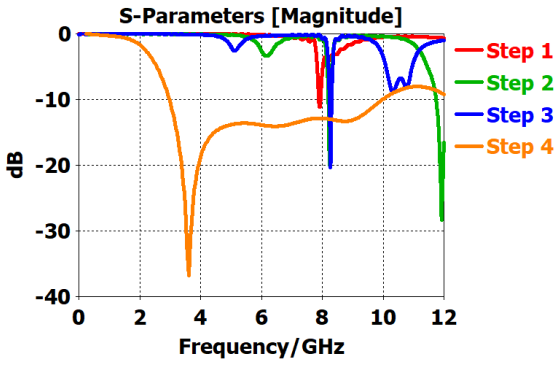

(b)

Figure. 3 Design stages and the corresponding S11 responses: (a) Antenna design steps and (b)S11 responses of design stages

At the final stage (step 4) the FGP is truncated to make a PGP keeping the three patches (EP1, EP2, EP3) connected together with the microstrip TL feed. A remarkable shift in the is seen in the spectrum. It is realized that the S11 is staying below -10 dB from 2.98 GHz reaching until 10 GHz. Once the wide band response is obtained, further analysis has been done to ensure the reliability and the quality of the design.

In Fig. 4(a), the reference port impedance and the Z-parameter are shown. It is observed that the port impedance is 50 Ω across the 2-12 GHz spectrum. As the feed width is calculated as 1.55 mm for the 50 Ω microstrip line, this result is expected and indicates a good match. Additionally, Fig. 4(a) shows that the antenna's imaginary impedance is close to zero at 3.5 GHz, while the real part is approximately 50 Ω. Similarly, other points where the 50 Ω line intersects correspond to lower values of the imaginary part.

Next, the antenna is connected to a vector network analyser (VNA) of model PNA-X N5242A from Agilent Technologies to measure the S11 response, with the setup illustrated in Fig. 4(b). Fig. 4(c) and (d) present the measured and simulated S11 and VSWR responses, respectively.

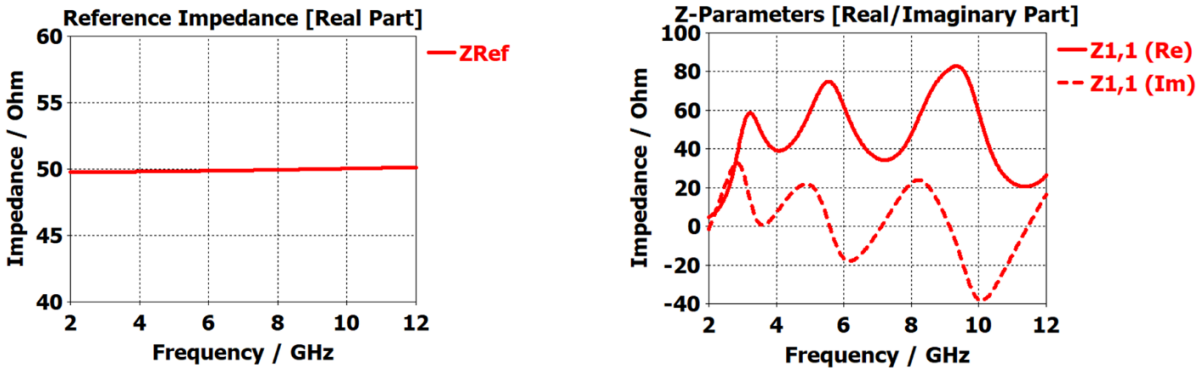

(a)

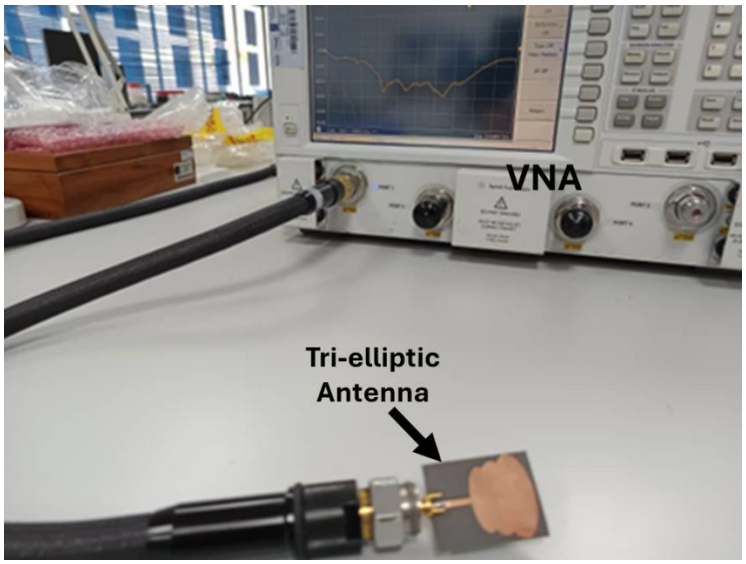

(b)

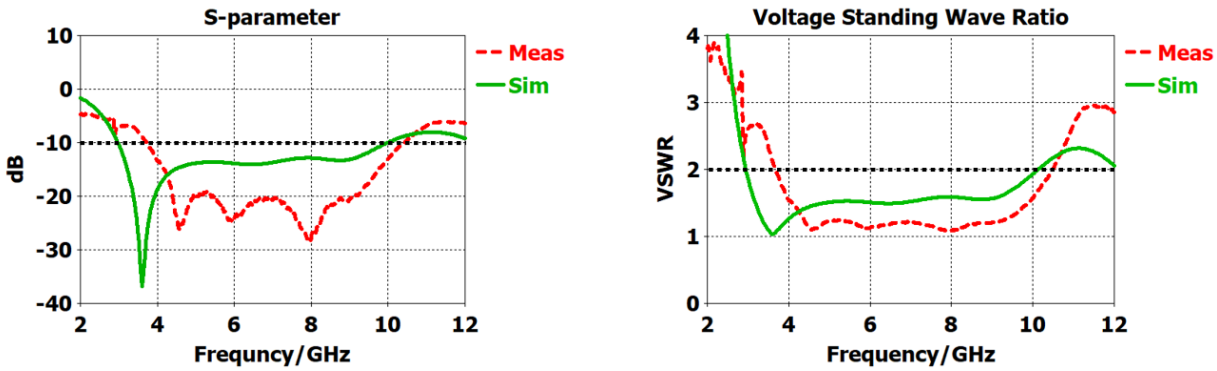

(c)S11 responses (d)VSWR

Figure. 4 The: (a) Reference impedance and the real & imaginary impedance, (b) S11 Measurement with VNA, (c) S11 responses and (d) VSWR

It is observed that the measured and simulated S11 responses are in good agreement. However, a deviation of approximately 700 MHz at the lower frequency side and 450 MHz at the higher frequency side of the bandwidth is noted. In simulation, the first -10 dB frequency point is observed at 2.98 GHz, while the measured value is shifted to 3.7 GHz. Similarly, the last -10 dB point in simulation occurs at 9.95 GHz, whereas the measured S11 value shifts to 10.4 GHz. The probable cause for this discrepancy as follows:

- Fabrication Tolerances: Variations in substrate thickness, trace widths, and gaps during fabrication process may lead to the final frequency deviating from the simulation.

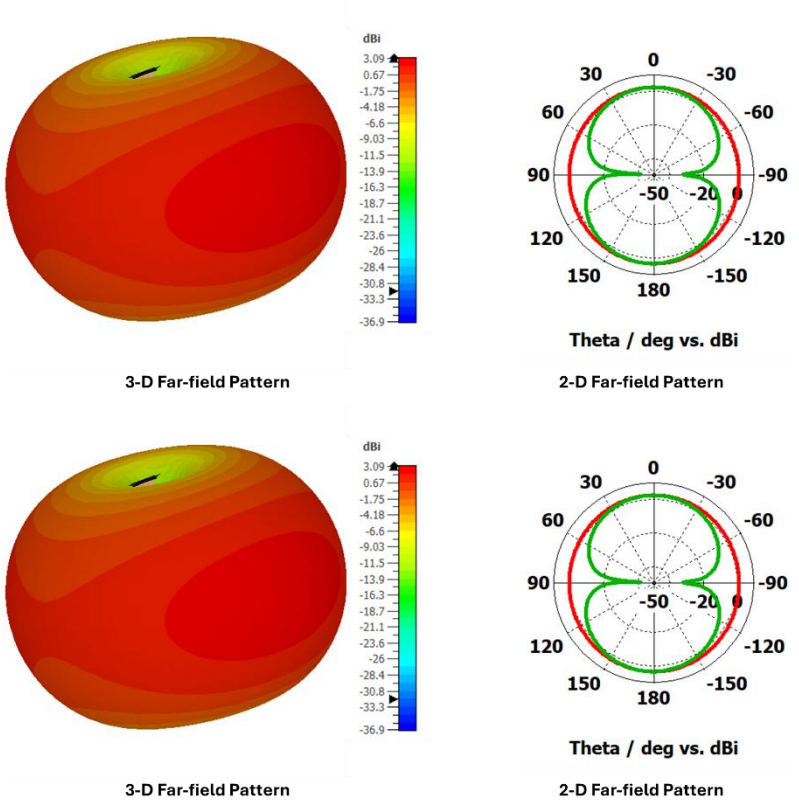

(a)

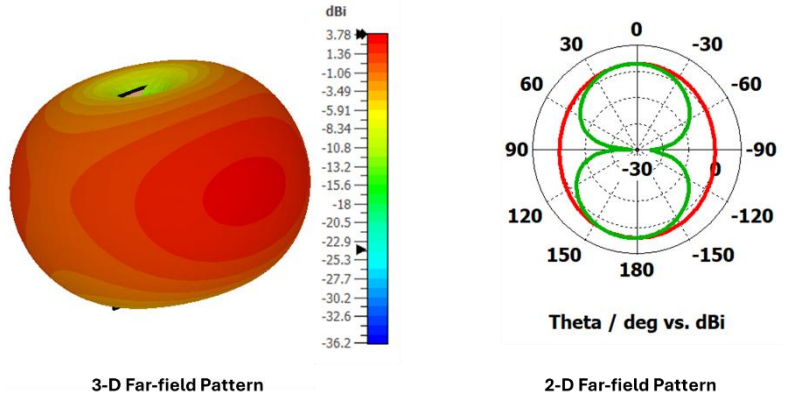

(b)

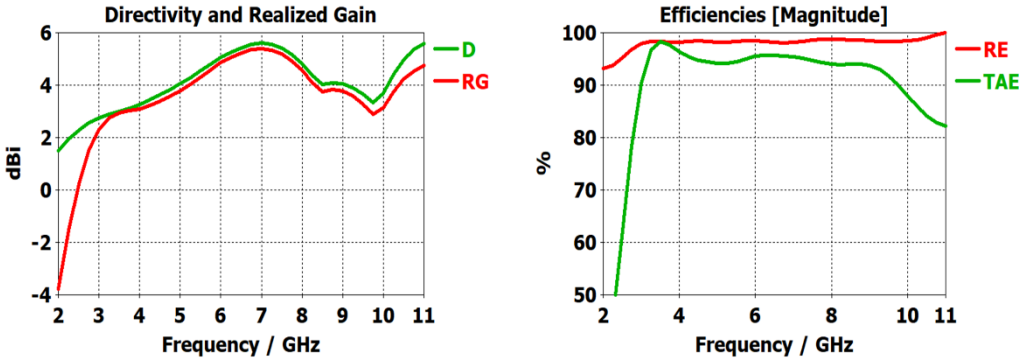

(c)

Figure. 5 The 3-D & 2-D radiation pattern, D, RG and the efficiencies: (a) 3-D and 2-D far-field patterns at 4 GHz, (b) 3-D and 2-D far-field patterns at 5 GHz, and (c) Directivity (D), Realized (RG), radiation efficiency (RE) and total antenna efficiency (TAE)

- Material Characteristics: The differences between actual and theoretical values of dielectric constants (ε_r) or loss tangents obtained from simulations can lead to another level of deviations. Besides, ambient conditions may also have effects on the material behaviour.
- Connectors and soldering: Misalignment of connectors may cause mismatches and shift in frequency. Also, irregular solder joints cause parasitic resistances and inductances and produce the similar effect.
- Experimental Inaccuracies: Issues in calibration or variable placement of the probes affects the precision. Moreover, the cables may radiate or reflect the signal, especially at high frequencies.

These can be overcome with a combination of accurate fabrication, detailed simulations, careful calibration, and reliable connectors and soldering techniques to minimize discrepancies.

Nonetheless, despite the deviation, the total -10 dB BW from the measured S11 is obtained as 6.7 GHz which is covering almost the entire UWB (3.1-10.6 GHz) region. Looking at the VSWR responses, it is observed that the measured BW for VSWR < 2 ranges from 3.67 to 10.5 GHz, increasing the available working bandwidth by an additional 130 MHz and extending the overall BW to 6.83 GHz. Both responses clearly justify the UWB nature of the proposed design.

Fig. 5 presents several key antenna parameters, including the 3-D and 2-D far-field radiation patterns, realized gain (RG) and directivity (D), as well as radiation efficiency (RE) and total antenna efficiency (TAE). Since the BW spans 3.67-10.5 GHz, the radiation patterns at 4 GHz and 5 GHz within the BW are selected for further analysis. Fig. 5(a) illustrate the 3-D and 2-D radiation patterns at 4 GHz. From the 3-D representation, it is observed that the primary radiation intensity (red) occurs in the horizontal plane of the antenna, while the vertical plane exhibits some nulls at the top and bottom of the antenna structure. This confirms the omnidirectional radiation pattern characteristic of the antenna. To further confirm this, 2-D slices of the horizontal (H-) plane (phi = 0) and the vertical/elevation (E-) plane (phi = 90) are plotted in Fig. 5(a). It is observed that the H-plane is nearly circular (uniform), while the E-plane exhibits two low-intensity (null) radiation points at theta = 90° and -90° cut angles. This scenario reinforces the omnidirectional nature of the far-field radiation pattern of the design. Similarly, Fig. 5(b) demonstrates a comparable scenario, further validating the omnidirectional characteristics of the proposed antenna at 5 GHz. Fig. 5(c) illustrates the realized gain (RG), directivity (D), radiation efficiency (RE), and total antenna efficiency (TAE) of the antenna. Eq. (4) shows the relationship between these parameters in decibels (dB). Where, η is the TAE of the antenna. It is realized from Fig. 5(c) that There is a slight difference between the directivity (D) and the realized gain (RG) of the proposed antenna, with the maximum values being 5.6 dBi for D and 5.4 dBi for RG at 7 GHz. Moreover, the GAR can be calculated at this frequency as 0.52 dBi/cm2. This indicates the comparatively high gain and high efficiency (low loss) characteristics of the proposed antenna with small size. To further support this observation, the radiation efficiency (RE) and total antenna efficiency (TAE) are also analysed, as shown in Fig. 5(c). The RE remains consistently high, exceeding 97% across the entire BW. Additionally, the TAE remains above 94% within the working BW, though it begins to decline beyond 9 GHz, reaching 85% at 10.5 GHz. Despite this slight reduction, the TAE maintains a consistently high value throughout the BW, reflecting the excellent quality and performance of the proposed design.

$$D_{dB} = RG_{dB} + \eta_{dB} \tag{4}$$

3. Real-world antenna validation

To perform the real-world validation this antenna is tested in three different scenarios: i) in the anechoic chamber for far field radiation pattern measurement, ii) validated through real-world LOS communication and iii) to check RFID suitability its validated with an existing CRFID multi-resonator. The subsequent subsections discuss the details.

3.1 Validation in anechoic chamber

Fig. 6 illustrates the setup of the far field radiation pattern measurement in anechoic chamber and the 2-D far field radiation pattern of the antenna at 4 and 5 GHz. Fig. 6(a) reveals the setup where the proposed antenna is used as Antenna Under Test (AUT) acting like a receiver (Rx) antenna. A fixed transmitter (Tx) horn antenna is placed at 4-meter distance to measure the 2-D radiation pattern. There is a camera to observe this operation from outside and the blue conical shaped spikes are absorbers made of sponge materials. Fig. 6(b) shows the 2-D E- and H-plane plots of the antenna at 4 and 5 GHz. It is seen that at both frequencies, the H-plane pattern is nominally circular as expected. Likewise, the E-plane is also showing a nominal bi-directional shape.

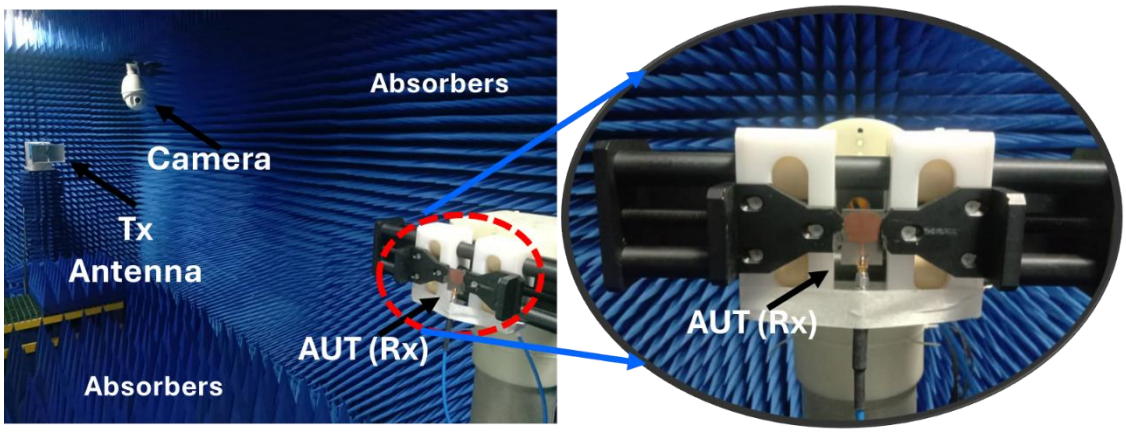

(a)

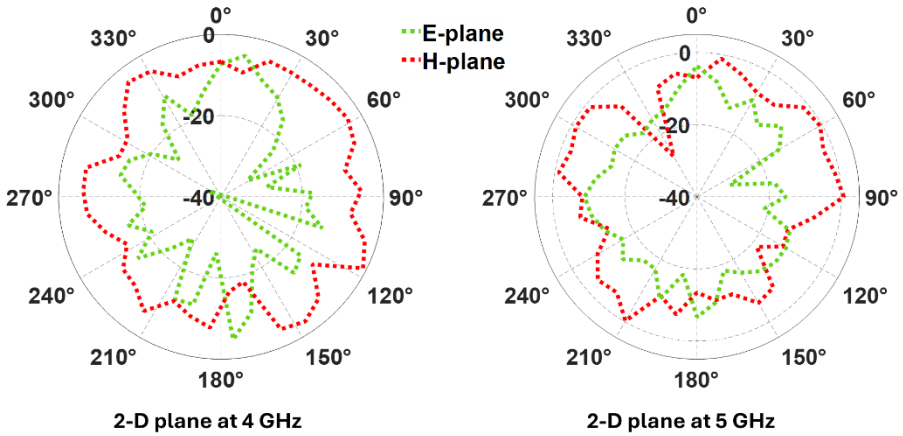

(b)

Figure. 6 Measurement setup in anechoic chamber and results at 4 and 5 GHz: (a)AUT in anechoic chamber and (b)The E- and the H-plane pattern at 4 and 5 GHz

Also, a slight discrepancy is visible as expected as imperfect nature of the measurement. Nevertheless, it can be concluded that the antenna is exhibiting the omni-directional far-field pattern.

3.2 Validation with LOS wireless communication

Similarly, the antenna is tested by establishing a Tx-Rx system to evaluate whether the proposed antenna can successfully receive the signal. The proposed antenna is used as the Rx antenna, while the Tx antenna is a pyramidal microwave horn with a working range of 0.8-18 GHz. Fig. 7 illustrates the setup for this validation. In this test, three scenarios are established for the proposed AUT (Rx) to perform line-of-sight (LOS) signal propagation with the Tx: (a) boresight, (b) orthogonal face, and (c) back side communication, as illustrated in Fig. 7(a), (b), and (c) respectively. In each scenario, a signal generator (SG) from Agilent (model no. N5183A) and a spectrum analyser (SA) from the same company (model no. CXA N9000A) are used to generate and receive the signal, respectively. The SG generates a transmitting signal level of +10 dBm at 5 GHz for each LOS validation setup. Two coaxial cables with SMA connectors are used at the Tx and Rx sides to connect the SG and SA to their respective antennas. The distance between the Tx and Rx antennas is maintained at 35 cm for all three scenarios.

In the case of boresight communication, it is found that the proposed antenna can successfully receive the transmitted signal. As seen on the SA's display (Fig. 7(a)), there is a single tone with a received signal strength level (RSSL) of -27.11 dBm at 5 GHz. Despite the gains of both Tx and Rx antennas, the reduced RSSL is expected due to the combined effects of path loss and cable losses. Similarly, from Fig. 7(b), for orthogonal (side) face communication, the RSSL is recorded as -29.52 dBm, with a loss of only 2.41 dB. Furthermore, for backside communication (Fig. 7(c)), the RSSL is measured at -26.23 dBm. As the antenna is omnidirectional, these results are justified, demonstrating that the antenna maintains a nominally uniform radiation pattern in all H-plane directions.

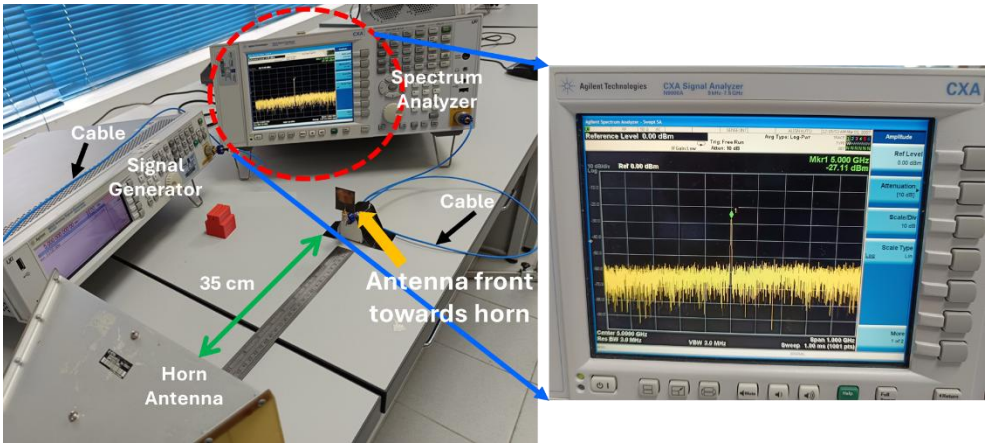

(a)

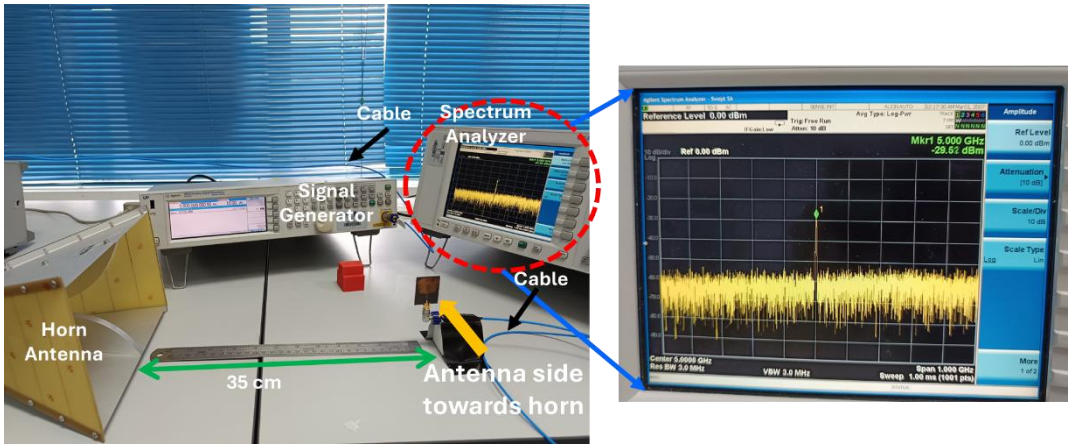

(b)

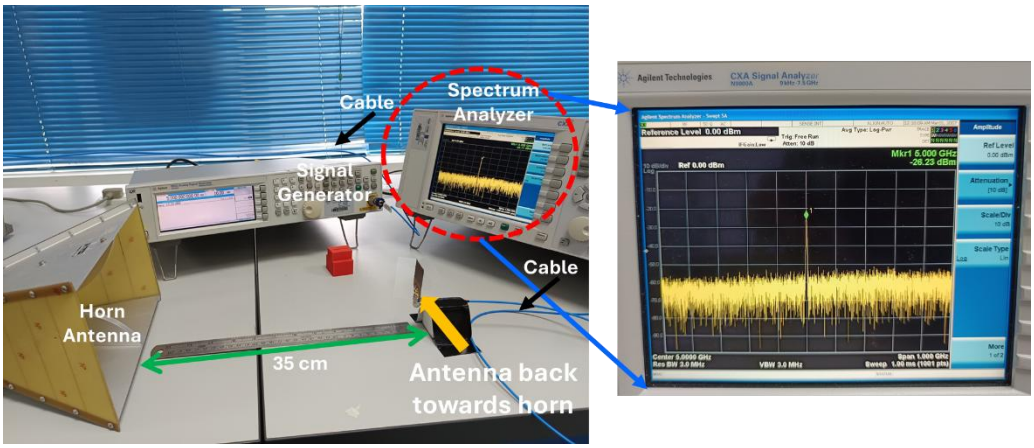

(c)

Figure. 7 Validation through LOS wireless communication: (a) Boresight communication, (b) Orthogonal face communication, and (c)Back side communication

Additionally, the front-to-back ratio is calculated to be approximately -0.88 dB, which is an excellent performance for an omnidirectional antenna. These findings clearly demonstrate that the proposed antenna is suitable for real-world multipath wireless communication scenarios. In the next section, this antenna is validated with a pre-existing CRFID multi-resonator.

3.3 Validation with CRFID multi-resonator

Fig. 8(a) illustrates setup for the validation of the existing 9-bit truncated-C multi-resonator (TCMR). On the right side, an enlarged (front & back) view of the 9-bit TCMR is also shown. The TCMR consists of 10 thin (0.3 mm) high-impedance lines, cascaded in parallel.

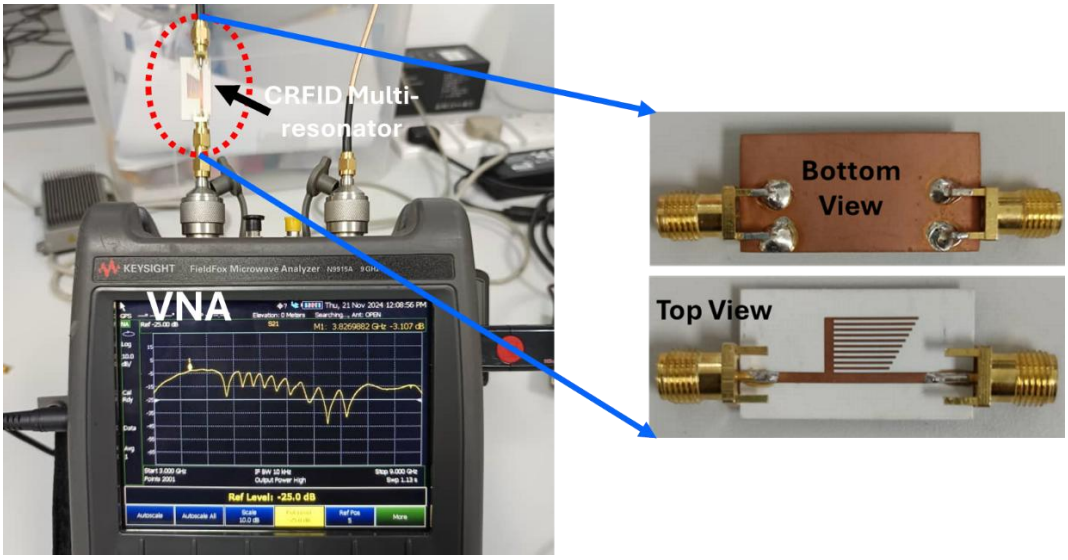

(a)

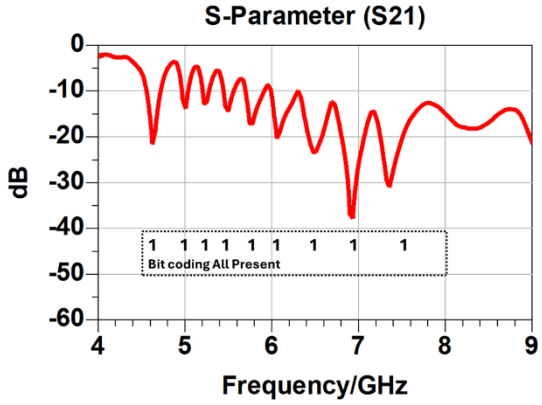

(b)

Figure. 8: (a) 9-bit TCMR validation with VNA and (b) S21 response with coding extraction

Additionally, the TCMR is connected in parallel with a 50 Ω TL and linked orthogonally to another 50 Ω TL of the same width. This 9-bit TCMR is fabricate on the substrate RO 3003c with $\varepsilon_r = 3, tan\delta = 0.0019$ and $h = 0.51mm$. Each pair of thin lines generates one bit of resonance in the spectrum. Therefore, to achieve 9 bits (9 resonances), 10 pairs of lines are required. Details of the TCMR design are provided in [23].

Fig. 8(b) shows the validation test setup for the TCMR using the same VNA. A two port S-parameter analysis is done. From the S21 response obtained from the VNA, it is evident that 9 distinct multi-resonance points appear in the spectrum. Typically, in chipless RFID (CRFID), bit coding is achieved using on-off keying (OOK) modulation, where the coding is determined based on the presence (1) or absence (0) of the resonators. In this case, all 9 resonators are present, resulting in a bit sequence of 111111111. As expected, all 9 dips are observed in the spectrum, confirming the extraction of the 'All One' bit sequence.

Next, the proposed antenna is tested with the TCMR to check that the bit sequence can be sent wirelessly by a sending (Tx) and a receiving (Rx) antenna pair. Two different fabricated proposed antenna copies are used and placed 2 cm apart to see the wireless communication. The setup is illustrated in Fig. 9(a). The TCMR, serving as the coding element, is attached to the Rx antenna and connected to Port 2 of the VNA. The second copy of the proposed antenna is used as the Tx antenna and connected to Port 1 of the VNA. The S21 response is shown in Fig. 9(b), with the S21 result from the previous Fig. 8(b) also included for benchmarking purposes. The data window is selected from 4-8 GHz, as all bits occur within this range.

From the results, it is evident that the bit stream/sequence of '111111111' can be clearly extracted in both cases. Additionally, the resonances are observed to occur at nearly the same points in the spectrum.

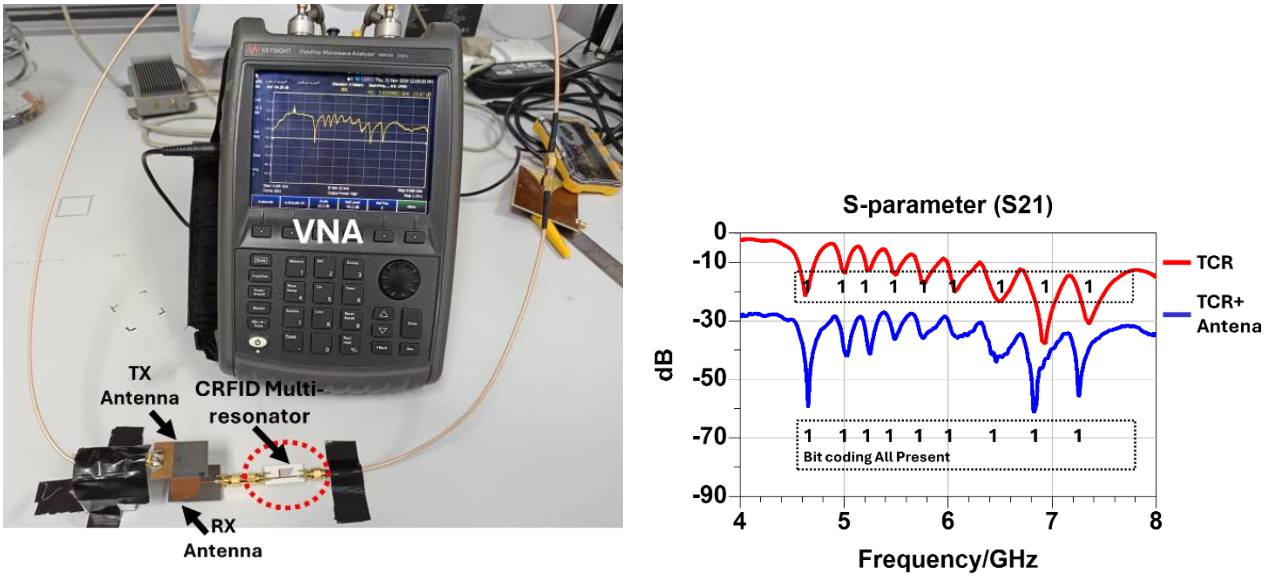

(a) (b)

Figure. 9: (a) Antenna test setup with TCMR and (b) S21 responses with coding validation

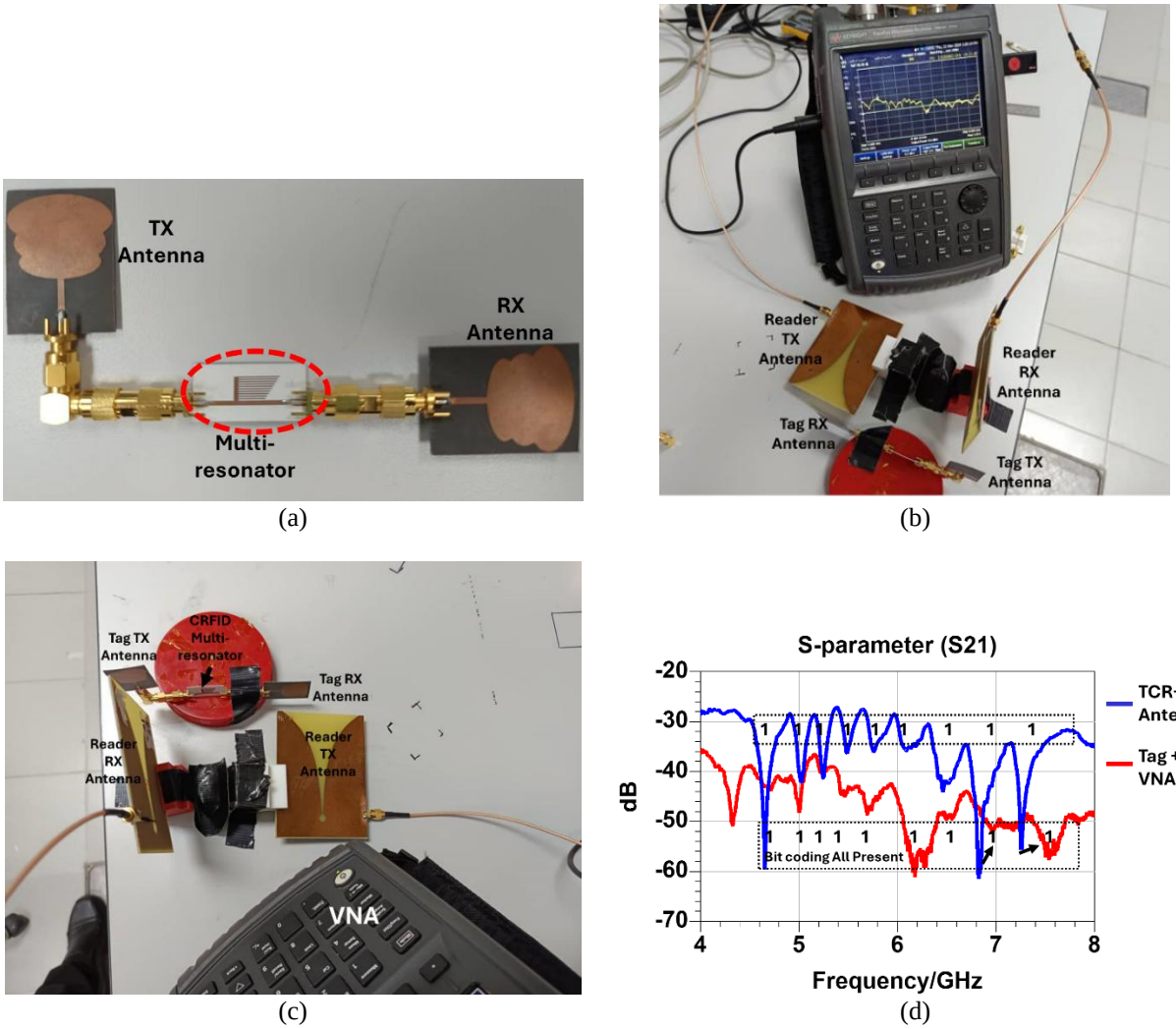

(a) (b)

(c) (d)

Figure. 10 The 9-bit TCMR CRFID Tag construction validation setup and the S21 responses with coding: (a) CRFID tag with the TCMR and proposed antennas, (b) Tag test setup (front view), (c) Setup top view, and (d) S21 responses with coding validation

However, a slight deviation in dB values is noticeable due to wireless path loss in the measurements. This setup demonstrates that the bit sequence can be successfully transmitted and extracted by the reader.

Fig. 10(a) illustrates the construction of the tag with the proposed antennas a 9-bit TCMR. The Tx and Rx are just different copies of the proposed antenna, and they are orthogonally placed to create polarization mismatch to mitigate crosstalk/interferences. Fig. 10(b) shows the real-world validation experimental setup (front view) of the tag (TCMR and antenna combined) with the reader (a VNA paired with two Vivaldi antennas). The Vivaldi antennas chosen in this setup as they are high-gain and well-suited for RFID reader applications. During the validation process, the CRFID tag is placed 2 cm away from the reader. Fig. 10(c) provides a top view of the setup. The S21 response is recorded and illustrated in Fig. 10(d), along with the previous test results described in Fig. 9(b) for benchmarking purposes. It is observed that, due to the wireless nature of the setup and the involvement of a retransmission-based bi-static detection method (which utilizes four antennas), the signal deviates slightly. In particular, the sharp dips in the spectrum are somewhat reduced.

It is also observed that for the 1st to 7th bits, the resonances occur at the same frequency points on the spectrum, albeit with reduced dips. For the 8th and 9th bits, the frequencies are slightly shifted compared to the experiment involving only two antennas. Nonetheless, the ‘All One’ bit stream (111111111) is still easily extracted. These results demonstrate that in both validation measurement setups, the desired bit stream can consistently and reliably be transmitted and received.

4. Conclusion

In conclusion, this paper presents a tri-elliptic-shaped microstrip patch antenna designed for UWB chipless RFID applications. The antenna is fabricated on a Rogers RT 5880 substrate and employs a partial ground plane to achieve UWB performance. Operating within the UWB frequency range of 3.67 to 10.5 GHz, it achieves a measured VSWR < 2 bandwidth of 6.83 GHz, a peak realized gain of 5.4 dBi, and a radiation efficiency exceeding 94% across the majority of the operating band. The compact structure, with dimensions of just 36.8 × 28 mm², incorporates three ellipses of varying dimensions to enhance bandwidth and minimize losses. Simulation and experimental results exhibit strong agreement, confirming the antenna's performance. This antenna exhibits This indicates a relatively high gain antenna with comparatively small in size. The antenna's functionality was further validated by integrating it with a 9-bit truncated-C multi-resonator (TCMR), enabling reliable wireless encoding and decoding of bit sequences. Real-world validation, including line-of-sight (LOS) and multipath scenarios, highlighted its robustness and suitability for wireless applications.

5. Future directions

While the tri-elliptic microstrip patch antenna has very promising performance for UWB chipless RFID applications, there are further challenges in the specific requirements of such industries as healthcare and logistics. In healthcare, antennas need to be dynamic, with wearability facing different operating conditions—placement on the human body, under conditions of bodily movement and changing skin conditions—demanding flexibility and biocompatibility for long-term usability. Correspondingly, logistic applications often require antennas that can withstand harsh environmental conditions such as high temperature, humidity, and mechanical stress related to transportation. Overcoming these challenges may mean using flexible substrates like polyimide or PET for wearable technology or durable materials like ceramic-filled PTFE to provide longevity in logistics. Reliability can be further increased by the application of protective coatings or moisture-resistant designs. By tackling these issues, the proposed antenna can be able to increase its usefulness further and place itself as a potential flexible solution for the different industry-based requirements.

Conflicts of Interest

The authors declare no conflict of interest.

Author Contributions

The contribution of the each authors are listed as follows: Conceptualization, Ghazi Bin Wan Mohamed and A. K. M. Zakir Hossain; methodology, A. K. M. Zakir Hossain; software, Ghazi Bin Wan Mohamed; validation, Ghazi Bin Wan Mohamed, Nurulhalim Bin Hassim, and Fahmida Hossain; formal analysis, Muhammad Ibn Ibrahimy; investigation, Ghazi Bin Wan Mohamed; resources, A. K. M. Zakir Hossain; data curation, Fahmida Hossain; writing—original draft preparation, Ghazi Bin Wan Mohamed; writing—review and editing, A. K. M. Zakir Hossain; visualization, Nurulhalim Bin Hassim; supervision, A. K. M. Zakir Hossain; project administration, Muhammad Ibn Ibrahimy; funding acquisition, Nurulhalim Bin Hassim.

Acknowledgments

The Fundamental Research Grant Scheme (FRGS) No. Ref fund this research: FRGS/1/2022/TK07/UTEM/03/8, provided by Ministry of Higher Education Malaysia (MOHE) and managed by Center for Research and Management (CRIM), Universiti Teknikal Malaysia Melaka (UTeM), Melaka Malaysia.

References

[1] M. N. Zahid, Z. Gaofeng, T. Sadiq, H. ur Rehman, and M. S. Anwar, "A Comprehensive Study of Chipless RFID Sensors for Healthcare Applications", *IEEE Access*, Vol. PP, p. 1, 2024, doi: 10.1109/ACCESS.2024.3446994.

[2] W. A. Indra, A. W. Y. Khang, Y. T. Yung, J. Abedalrahim, and J. Alsayaydeh, "Radio-frequency identification (RFID) item finder using radio frequency energy harvesting", *ARPN J. Eng. Appl. Sci.*, Vol. 14, No. 20, pp. 3554-3560, 2019.

[3] A. K. M. Z. Hossain, M. I. Ibrahimy, and S. M. A. Motakabber, "Spiral resonator for ultra wide band chipless RFID tag", In: *Proc. of 5th Int. Conf. Comput. Commun. Eng. Emerg. Technol. via Comp-Unication Converg*, pp. 281-283, 2015, doi: 10.1109/ICCCE.2014.86.

[4] S. Preradovic *et al.*, "Multiresonator-Based Chipless RFID System", *IEEE Trans. Microw. Theory Tech.*, Vol. 57, No. 5, pp. 1411-1419, 2009.

[5] A. K. M. Z. Hossain, S. M. A. Motakabber, and M. I. Ibrahimy, "Microstrip Spiral Resonator for the UWB Chipless RFID Tag", *Adv. Intell. Syst. Comput.*, Vol. 1089, pp. 355-358, 2015, doi: 10.1007/978-3-319-08422-0_52.

[6] S. Preradovic, S. Roy, and N. Karmakar, "Fully printable multi-bit chipless RFID transponder on flexible laminate", In: *Proc. of APMC 2009 - Asia Pacific Microw. Conf. 2009*, pp. 2371-2374, 2009, doi: 10.1109/APMC.2009.5385460.

[7] P. Prabavathi and S. Subha Rani, "Modified microstrip transmission line based chipless RFID tag with high bit encoding", *Meas. J. Int. Meas. Confed.*, Vol. 190, No. November 2020, p. 110684, 2022, doi: 10.1016/j.measurement.2021.110684.

[8] R. Vijay, V. Ramasamy, M. Selvaraj, R. Anbazhagan, and A. Rengarajan, "Development of low-profile spectral signature chipless flexible RFID prototype for 5G supply chain IoT applications", *Eng. Sci. Technol. an Int. J.*, Vol. 36, p. 101296, 2022, doi: 10.1016/j.jestch.2022.101296.

[9] X. Nie, N. Wu, C. T. M. Wu, and P. Y. Chen, "A Compact, Batteryless, and Chipless Intermodulation Sensor for Wireless Crack Detection", *IEEE Sens. J.*, Vol. 24, No. 7, pp. 9998-10005, 2024, doi: 10.1109/JSEN.2024.3368332.

[10] A. K. M. Zakir Hossain, W. A. Indra, J. A. Jamil Alsayaydeh, and S. G. Herawan, "A Planar Monopole UWB Antenna with Partial Ground Plane for Retransmission-Based Chipless RFID", *Int. J. Intell. Eng. Syst.*, Vol. 14, No. 4, pp. 539-547, 2021, doi: 10.22266/ijies2021.0831.47.

[11] N. Saranya, T. Deepa, P. Raja, K. Paayal, A. Sofiya, and R. Swetha, "A Low Profile 20-Bit Frequency-Coded L-Shape Multi-Slot Resonator for Chipless RFID Applications", *Prog. Electromagn. Res. C*, Vol. 149, No. September, pp. 105-109, 2024, doi: 10.2528/PIERC24090202.

[12] R. E. Ghiri and K. Entesari, "A 50.7-Bit Retransmission-Based Chipless RFID Tag with Miniaturized Resonators", In: *Proc. of 2021 IEEE Top. Conf. Wirel. Sensors Sens. Networks, WiSNeT 2021*, pp. 12-14, 2021, doi: 10.1109/WiSNeT51848.2021.9413790.

[13] J. Hu, Y. Xie, G. Wan, and L. Xie, "A Novel Anti-Interference Encapsulated 3-Bit Coded RFID Humidity Sensor Based on Bent Microstrip", *IEEE Trans. Instrum. Meas.*, Vol. 73, pp. 1-10, 2024, doi: 10.1109/TIM.2024.3398133.

[14] H. A. Malhat, E. A. El-Refaay, and S. H. Zainud-Deen, "Temperature sensor integrated curl resonator chipless RFID tag for high capacity data identification applications", *Microsyst. Technol.*, Vol. 29, No. 1, pp. 157-168, 2023, doi: 10.1007/s00542-022-05401-w.

[15] R. Raju and G. E. Bridges, "A Compact Wireless Passive Harmonic Sensor for Packaged Food Quality Monitoring", *IEEE Trans. Microw. Theory Tech.*, Vol. 70, No. 4, pp. 2389-2397, 2022, doi: 10.1109/TMTT.2022.3142063.

[16] S. K. Gupta, S. Kumar, and A. Sharma, "A Miniaturized Dual-Resonator-Based High-Capacity Chipless Radio Frequency Identification Tag Sensor", *IEEE Sensors Lett.*, Vol. 6, No. 11, pp. 1-4, 2022, doi: 10.1109/LSENS.2022.3218503.

[17] W. M. Abdulkawi, N. Nizam-Uddin, A. F. A. Sheta, I. Elshafiey, and A. M. Al-Shaalan, "Towards an efficient chipless rfid system for modern applications in iot networks", *Appl. Sci.*, Vol. 11, No. 19, 2021, doi:

10.3390/app11198948.

[18] B. Aslam, M. A. Azam, Y. Amin, J. Loo, and H. Tenhunen, "A high capacity tunable retransmission type frequency coded chipless radio frequency identification system", *Int. J. RF Microw. Comput. Eng.*, Vol. 29, No. 9, pp. 1-11, 2019, doi: 10.1002/mmce.21855.

[19] M. E. Bin Jalil, M. K. A. Rahim, N. A. Samsuri, and N. A. Murad, "Miniaturized And Wideband Chipless RFID Tag Antenna", In: *Proc. of 2021 Int. Symp. Antennas Propagation, ISAP 2021*, pp. 1-2, 2021, doi: 10.23919/ISAP47258.2021.9614547.

[20] A. K. M. Zakir Hossain, N. Bin Hassim, J. A. J. Alsayaydeh, M. K. Hasan, and M. R. Islam, "A Tree-profile Shape Ultra Wide Band Antenna for Chipless RFID Tags", *Int. J. Adv. Comput. Sci. Appl.*, Vol. 12, No. 4, pp. 546-550, 2021, doi: 10.14569/IJACSA.2021.0120469.

[21] Y. Ren, N. Wu, K. C. Chang, Y. S. Su, and P. Y. Chen, "A Zero-Power Harmonic Tag for Real-Time Wireless Food Quality Monitoring", *IEEE Sensors Lett.*, Vol. 8, No. 7, pp. 1-4, 2024, doi: 10.1109/LSENS.2024.3416084.

[22] M. S. Islam, M. I. Ibrahimy, S. M. A. Motakabber, A. K. M. Z. Hossain, and S. M. K. Azam, "Microstrip patch antenna with defected ground structure for biomedical application", *Bull. Electr. Eng. Informatics*, Vol. 8, No. 2, pp. 586-595, 2019, doi: 10.11591/EEI.V8I2.1495.

[23] A. K. M. Z. Hossain, M. I. Ibrahimy, S. M. A. Motakabber, S. M. K. Azam, and M. S. Islam, "Multi-resonator application on size reduction for retransmission-based chipless RFID tag", *Electron. Lett.*, Vol. 57, No. 1, pp. 26-29, 2021, doi: 10.1049/ell2.12036.